Structural Basis for CO_2 Fixation by a Novel Member of the Disulfide Oxidoreductase Family of Enzymes, 2-Ketopropyl-Coenzyme M Oxidoreductase/Carboxylase[†,‡]

Boguslaw Nocek,[§] Se Bok Jang,[⊥,§] Mi Suk Jeong,[⊥,§] Daniel D. Clark,[∥] Scott A. Ensign,[∥] and John W. Peters*[,§]

Department of Chemistry and Biochemistry, Montana State University, Bozeman, Montana 59717, and Department of Chemistry and Biochemistry, Utah State University, Logan, Utah 84322

Received August 6, 2002; Revised Manuscript Received September 9, 2002

ABSTRACT: The NADPH:2-ketopropyl-coenzyme M oxidoreductase/carboxylase (2-KPCC) is the terminal enzyme in a metabolic pathway that results in the conversion of propylene to the central metabolite acetoacetate in *Xanthobacter autotrophicus* Py2. This enzyme is an FAD-containing enzyme that is a member of the NADPH:disulfide oxidoreductase (DSOR) family of enzymes that include glutathione reductase, dihydrolipoamide dehydrogenase, trypanothione reductase, thioredoxin reductase, and mercuric reductase. In contrast to the prototypical reactions catalyzed by members of the DSOR family, the NADPH: 2-ketopropyl-coenzyme M oxidoreductase/carboxylase catalyzes the reductive cleavage of the thioether linkage of 2-ketopropyl-coenzyme M, and the subsequent carboxylation of the ketopropyl cleavage product, yielding the products acetoacetate and free coenzyme M. The structure of 2-KPCC reveals a unique active site in comparison to those of other members of the DSOR family of enzymes and demonstrates how the enzyme architecture has been adapted for the more sophisticated biochemical reaction. In addition, comparison of the structures in the native state and in the presence of bound substrate indicates the binding of the substrate 2-ketopropyl-coenzyme M induces a conformational change resulting in the collapse of the substrate access channel. The encapsulation of the substrate in this manner is reminiscent of the conformational changes observed in the well-characterized CO_2-fixing enzyme ribulose 1,5-bisphosphate carboxylase/oxidase (Rubisco).

Aerobic microorganism *Xanthobacter* strain Py2 is one of several bacteria that have been shown to be capable of utilizing short chain aliphatic alkenes as a sole source of carbon and energy (*1*−*3*). The pathways for the bacterial metabolism of propylene have been extensively studied in both *Xanthobacter autotrophicus* strain Py2 as well as the actinomycete *Rhodococcus rhodochrous* strain B276 (*4*−*6*). The conversion of propylene to an enantiomeric excess of (*R*)-epoxypropane is catalyzed by a di-Fe-containing alkene monoxygenase (*7*) that is similar in some ways to the structurally characterized methane monoxygenase from the methanotroph *Methylococcus capsulatus* Bath (*8*). The subsequent conversion of both enantiomers of epoxypropane to acetoacetate occurs by a three-step pathway consisting of four enzyme components (*6*). A significant finding in defining the enzymology of the pathway was the recent discovery that epoxide metabolism in *Xanthobacter* involves the cofactor coenzyme M (*9*). Coenzyme M (CoM)[1] was until that time believed to be restricted to the methanogenic archaebacteria.

The first step results in the conjugation of CoM to (*R*)- or (*S*)-epoxypropane, forming the corresponding enantiomer of 2-hydroxypropyl-CoM. In the next step, two stereospecific short chain dehydrogenases catalyze the oxidation of the individual enantiomers of 2-hydroxypropyl-CoM, yielding the common intermediate 2-ketopropyl-CoM (*9*, *10*). The final step in the pathway is conversion of 2-ketopropyl-CoM to acetoacetate with concomitant regeneration of free CoM. This pathway represents a clever and unprecedented strategy for converting highly reactive epoxides to central metabolites for use as the primary carbon and energy source of the bacteria.

As a part of our ongoing interest in the enzymology of this pathway, we have been studying the properties of the enzyme that catalyzes the terminal CO_2-fixing step (Figure

[†] This work was supported by National Science Foundation Grant MCB-0110269 (to J.W.P.) and National Institutes of Health Grant GM51805 (to S.A.E.). The data collection facility at SSRL is funded by the U.S. Department of Energy, Office of Basic Energy Sciences, and by the NIH Biomedical Research Technology Program, Division of Research Resources. J.W.P. is the recipient of a Camille Dreyfus Teacher/Scholar Award.

[‡] Coordinates for the native and substrate-bound states of 2-ketopropyl-coenzyme M oxidoreductase/carboxylase are deposited in the Protein Data Bank as entries 1MOK and 1MO9, respectively.

* To whom correspondence should be addressed. Phone: (406) 994-7211. Fax: (406) 994-7212. E-mail: john.peters@chemistry.montana.edu.

[⊥] Present address: Korea Institute of Nanobiotechnology Pusan National University, Pusan 609-735, Korea.

[§] Montana State University.

[∥] Utah State University.

[1] Abbreviations: 2-hydroxypropyl-CoM, 2-[(2-hydroxypropyl)thio]-ethanesulfonate; 2-KPCC, NADPH-dependent 2-ketopropyl-CoM oxidoreductase/carboxylase; 2-KCoM, 2-ketopropyl-CoM {2-[(2-ketopropyl)-thio]ethanesulfonate}; CoM, coenzyme M (2-mercaptoethanesulfonate); DSOR, NADPH:disulfide oxidoreductase; Rubisco, ribulose 1,5-biphosphate carboxylase/oxidase; MIRAS, multiple isomorphous replacement and anomalous scattering.

10.1021/bi026580p CCC: $22.00
Published on Web 10/05/2002

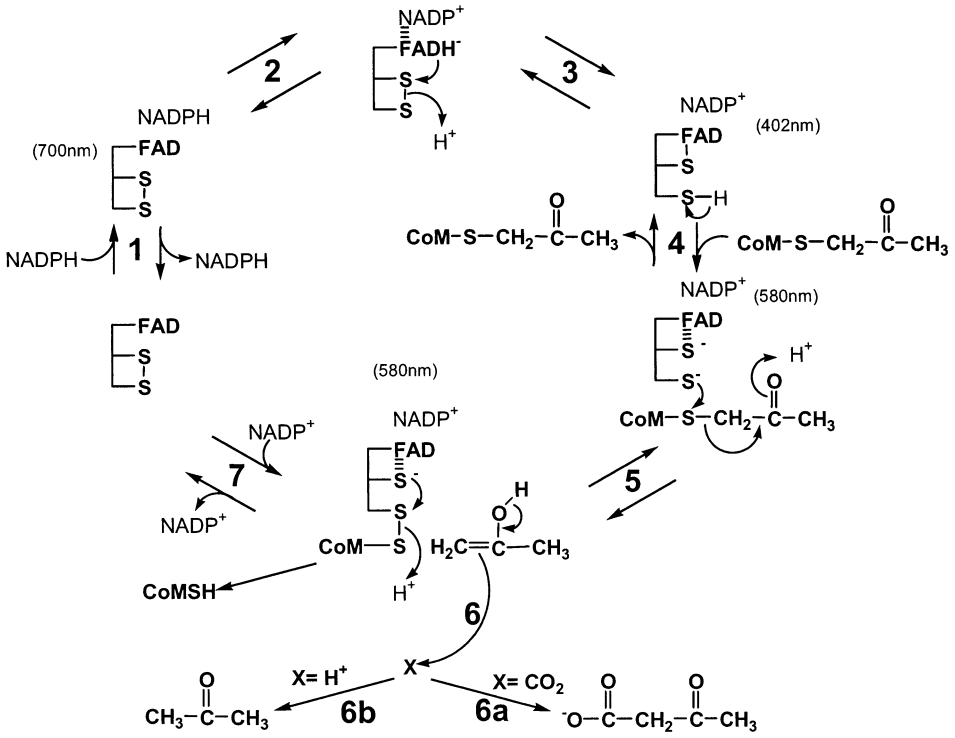

FIGURE 1: Proposed catalytic cycle for 2-KPCC. The mechanism of 2-ketopropyl-CoM reduction and carboxylation is based on the results of biochemical and kinetic studies of the enzyme (*10*, *13*) and the structural insights provided herein. The numbers refer to the steps of the catalytic cycle, with steps 6a and 6b representing the alternate protonation and carboxylation, respectively, of the enolacetone intermediate. The figure was adapted from Figure 6 from Clark et al. (*10*).

1). This enzyme, an NADPH:2-ketopropyl-CoM oxidoreductase/carboxylase (2-KPCC), is a unique member of the FAD-containing NAD(P)H dependent disulfide oxidoreductase family of enzymes as determined by primary sequence similarities and biochemical properties (*6*, *9*−*13*). Several members of this enzyme family (*14*) have been structurally characterized, including glutathione reductase, dihydrolipoamide dehydrogenase, and thioredoxin reductase. The catalytic activity of these enzymes has been described as involving two half-reactions (*14*−*17*). The first half-reaction involves the transfer of reducing equivalents from pyridine nucleotides via flavin adenine dinucleotide to a cysteine that is almost always a component of a disulfide bond. The second half-reaction involves the reduction of substrate and regeneration of the enzyme disulfide. There are several key differences in the biochemical reaction catalyzed by 2-KPCC in comparison to those with other members of the DSOR family. As shown in Figure 1, 2-KPCC catalyzes a thioether bond cleavage, as opposed to the disulfide bond cleavage catalyzed by glutathione reductase, trypanothione reductase, and dihydrolipoamide dehydrogenase (*14*). Even more notable, however, is the subsequent carboxylation reaction catalyzed by the enzyme. The α-carbanion produced as a result of thioether bond cleavage has been shown to follow one of two fates enzymatically: protonation to form acetone when CO_2 is excluded from the enzyme or carboxylation in the presence of CO_2 to form acetoacetate. In terms of the metabolism of the organism, the formation of acetoacetate is advantageous, and in the presence of carbon dioxide, little or no acetone is formed (*10*). Of particular interest in our analysis is the structural basis for the mechanism by which the enzyme discriminates between carbon dioxide and protons readily available from the bulk solvent.

The three-dimensional structure of 2-KPCC has been determined by the multiple isomorphous replacement and anomalous scattering (MIRAS) method and refined to 1.65 Å resolution. The structure of 2-KPCC in the presence of the substrate 2-ketopropyl-CoM reveals a genuinely unique member of the DSOR family and provides significant insights into how this enzyme coordinates reductive cleavage of the thioether bond with carboxylation.

EXPERIMENTAL PROCEDURES

Crystals of 2-KPCC in the native state and in the presence of the substrate 2-ketopropyl-CoM were obtained as described previously (*18*). The crystals of 2-KPCC in the presence of the substrate 2-ketopropyl-CoM (2-KCoM) belong to monoclinic space group $P2_1$ with one dimer per asymmetric unit with the following unit cell dimensions: $a = 88.0$ Å, $b = 60.1$ Å, $c = 105.6$ Å, and $\beta = 102.5°$. The data from the crystals grown in the absence of substrate or product can only be reduced in triclinic space group $P1$ with the following unit cell dimensions: $a = 65.6$ Å, $b = 87.5$ Å, $c = 100.7$ Å, $\alpha = 72.0°$, $\beta = 73.4°$, and $\gamma = 69.8°$. Although the primary sequence is considerably identical with the sequences of members of the DSOR family, attempts to determine the structure using molecular replacement methods were unsuccessful in either crystal form. The structure was determined by the method of multiple isomorphous replacement and anomalous scattering using four weak heavy atom derivatives. All derivatives with the exception of Xe were prepared by soaking the crystals with heavy atom reagents at a concentration of 5−10 mM for 5−21 h prior to data collection (Table 1). The Xe derivative was prepared using the Xe pressure cell at the Stanford Synchrotron Radiation Laboratory (SSRL) (*19*). Substrate-bound and three deriva-

Table 1: Data Collection and Structure Determination Statistics

	native	native with 2-KCoM	10 mM EMP, 21 h	5 mM EMTS, 21 h	400 psi Xe, 2 m	4 mM $TlCl_3$, 7 h
data statistics						
resolution (Å)	2.80	1.64	3.50	2.80	2.95	2.95
no. of observed reflections	213523	504165	41012	88322	54964	53957
no. of unique reflections	48234	164972	14026	24756	20533	20070
R_{merge}[a] (%)	9.8	6.7	10.7	12.9	6.7	3.3
completeness (%)	92.1	98.2	91.7	98.7	89.2	88.6
I/σ	10.9	7.8	11.5	9.7	6.1	16.0
MIRAS statistics (resolution range of 20.0−4.0 Å)						
R_C[b]			0.59	0.66	0.69	0.74
F_H/E[c]			1.02	0.83	0.56	0.54

[a] $R_{merge} = \sum_{hkl}\sum_i|I_i - \langle I\rangle|/\sum_{hkl}\sum_i|\langle I\rangle|$, where I_i is the intensity for the ith measurement of an equivalent reflection with indices h, k, and l. [b] $R_C = \sum_{hkl}||F_{PH} \pm F_P| - F_H(\text{calc})|/\sum_{hkl}|F_{PH} \pm F_P|$. [c] $F_H/E = (\sum_n|F_H|^2/\sum_n|E|^2)^{1/2}$ where $\sum_n|E|^2 = \sum_n[|F_{PH}|(\text{obs}) - |F_{PH}|(\text{calc})]^2$.

tive data sets [ethylmercurithiosalicylic acid (EMTS), Xe, and $TlCl_3$] were collected at SSRL beam line 9-1 equipped with a mar345 imaging plate detector (MarUSA, Inc.). Native data and data for the remaining heavy atom derivative [ethylmercuric phosphate (EMP)] were collected with a Rigaku rotating anode X-ray generator producing Cu Kα radiation equipped with an Raxis-IIc imaging plate area detector (Molecular Structure Corp., The Woodlands, TX). Data sets were processed with MOSFLM (*20*) or DENZO (*21*) and scaled with either SCALPACK (*21*) or SCALA of the CCP4 program suite (*22*).

The positions of multiple heavy atom binding sites were identified using SOLVE (*23*), resulting in a figure of merit of 0.53 from 20.0 to 4.0 Å resolution (Table 1). The heavy atom sites were utilized to identify noncrystallographic 2-fold operation and resulted in a significant improvement in the phases and an overall figure of merit of 0.72. Interpretable MIRAS electron density maps were obtained upon 2-fold averaging and phase extension to the full resolution range of the data (20.0−1.65 Å) using the density modification (DM) routine of the CCP4 suite (*22*), resulting in a final figure of merit of 0.75. These initial experimental phase-extended maps were sufficient to position polypeptide residues from position 70 to 420 using the model building program O (*24*). The partial model was then utilized for phase combination and automated model building and map improvement using ARP/wARP (*25*, *26*), resulting in excellent map quality and allowing fitting of the remainder of the model. The structure refinement was carried out using CNS (*27*) from 20 to 1.65 Å with a 0σ cutoff with 5% of the data set aside for the calculation of R_{free} (*28*). The structure of the native enzyme was determined by molecular replacement by EPMR (*29*) using the structure of the substrate-bound enzyme as a search model. A solution with two dimers in the asymmetric unit resulted in a correlation coefficient of 0.401 and an *R* factor of 0.478 with reasonable protein packing interactions. A well-determined structure was obtained through multiple rounds of model building using the program O (*24*) followed by refinement using CNS (*27*) using data from 20.0 to 2.8 Å resolution with a 0.5σ cutoff (Table 2).

The results of the refinement are given in Table 1. The final structural models obey reasonable stereochemistry with 100% of the residues occupying allowed regions of a Ramachandran plot calculated using PROCHECK (*30*). All figures were generated using SWISS PDB VIEWER (*31*).

Table 2: Refinement Statistics

	native	native with 2-KPCoM
resolution range (Å)	20.0−2.80	20.0−1.65
R_{cryst}	0.224	0.187
R_{free}	0.276	0.213
no. non-hydrogen atoms		
protein	8046	8046
cofactor/substrate	106	128
solvent	0	999
rmsd from target values		
bond lengths (Å)	0.010	0.005
bond Angles (deg)	1.8	1.3
average isotropic B factors (Å^2)		
protein main chain	35.9	16.0
protein side chain	32.7	16.0
FAD	29.5	12.7
2-ketopropyl-CoM	−	19.1

RESULTS AND DISCUSSION

Overall Structure. The overall structure of 2-KPCC is very similar to the dimeric structures observed for the classic members of the DSOR family (*14*, *15*) (Figure 2A,B), including glutathione reductase (*32*−*35*), trypanothione reductase (*36*), and lipoamide dehydrogenase (*37*). Each monomer can be divided into three domains, including the FAD binding domain, the NADPH binding domain, and the dimerization or, as it has been previously termed, interface domain (*14*). The FAD and NADPH binding domains are standard Rossmann nucleotide binding structural motifs of large twisted β-sheets surrounded by α-helices. The FAD domain consists of a seven-stranded mixed β-sheet surrounded by four α-helices and a small three-stranded antiparallel β-sheet at a 45° angle. The NADPH domain is similar to the FAD domain, consisting of a five-stranded parallel β-sheet with two short α-helices and a small three-stranded β-sheet at a 45° angle with respect to the main β-sheet. These two domains are linked by two crosses of the main chain and a long α-helix which spans both domains and lies adjacent to the interface domains of both subunits. The third domain has been termed the interface domain and provides a significant amount of the intersubunit contacts that stabilize the dimer. The interface domain is also mainly β in structure; however, it is α-helices that flank the central β-sheet that form a number of the specific interactions between the subunits. The three domains make up two interlocked L-shaped monomers having the interface domain of one subunit interacting with both the interface domain and the FAD domain of the opposing subunit.

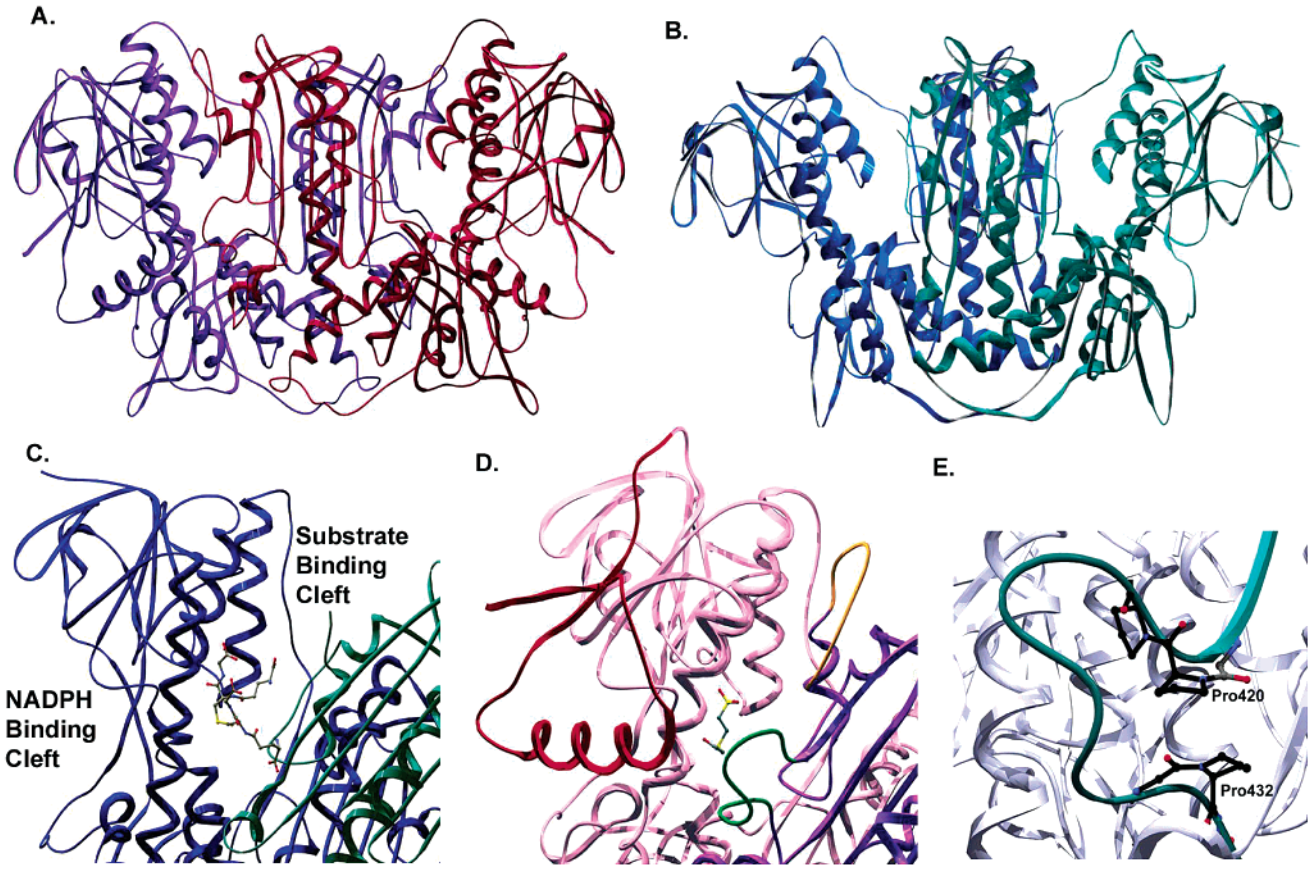

FIGURE 2: (A) Overall fold of the dimeric 2-KPCC with individual subunits colored in dark red and magenta. (B) Overall fold of the well-characterized glutathione reductase in the same orientation as the structure of 2-KPCC shown in panel A with the individual subunits shown in green and blue. (C) Substrate binding cleft region of glutathione reductase with the bound glutathione substrate. (D) Analogous substrate binding cleft of 2-KPCC with bound 2-ketopropyl-CoM. The regions of 2-KPCC observed to occupy the cleft are shown by N-terminal region in red supplied by one subunit of the dimer and a C-terminal region in yellow and insertion region in green from the second subunit of the dimer. (E) Close-up of the unique insertion region showing three proline residues which allow the tight looping of the region. The two proline residues which signify the termini of the insertion are found to be in the *cis* conformation.

The NADPH and FAD binding domains are oriented such that both nucleotide binding sites are located at the interface of these two nucleotide binding domains. The NADPH binding cleft is located between the FAD and NADPH binding domains, and is to the largest extent analogous to the other members of the family such that docking of NADPH into the site in 2-KPCC allows the rationalization of interactions similar to that observed for other members of the DSOR family.

Substrate Binding Cleft. Substrate access in the other dimeric members of the DSOR family is defined by a large open cleft that separates the FAD domain of one monomer of the dimer and the interface domain of the other monomer of the dimer. The redox active disulfide is located at the base of the cleft. For the majority of these enzymes, the reaction path involves the reductive cleavage and protonation of the substrate with protons presumably supplied from the bulk solvent. An open cleft allows easy access for substrate binding and release, providing a continuous source of protons from the bulk solvent (Figure 2C). Access to the substrate binding site of 2-KPCC is distinct from all other members of the family. In comparison to other members of the family, 2-KPCC has notable differences at the N- and C-termini and a 13-amino acid insertion within the interface domain. The three additional regions of 2-KPCC in concert occupy the large substrate access cleft observed in the other dimeric members of the family (Figure 2D). The N-terminal region which forms one of the peripheral β-strands of the central β-sheet of the FAD domain and an α-helix contacts the insertion within the interface domain, effectively blocking the large cleft observed in the other dimeric members of the family. Interestingly, the inserted region is flanked by two *cis*-proline residues (Pro420 and Pro432) which approach each other very closely (Figure 2E). In the substrate-bound form of 2-KPCC, 2-ketopropyl-CoM is virtually buried within the protein such that a substrate access channel is not discernible. Access to the substrate binding site is limited to a narrow hydrophobic channel.

Substrate Binding Site. The substrate is bound by specific interactions with CoM. The sulfonate moiety of CoM is bound by two Arg side chains (Arg56 and Arg365) which approach from the sides and interact directly with additional side chain and main chain atoms through hydrogen bonding (Figure 3A). The Arg side chains approach from the sides, and an adjacent phenylalanine side chain (Phe57) acts as a "backstop" preventing further translation of the substrate and thus allowing proper alignment of the thioether linkage with respect to the enzyme disulfide for reductive cleavage (Figure 3B). Reductive cleavage occurs when NADPH initiates the reduction pathway through direct hydride transfer to the isoalloxazine ring of FAD. The binding site for NADPH is a large cleft at the interface between the two nucleotide

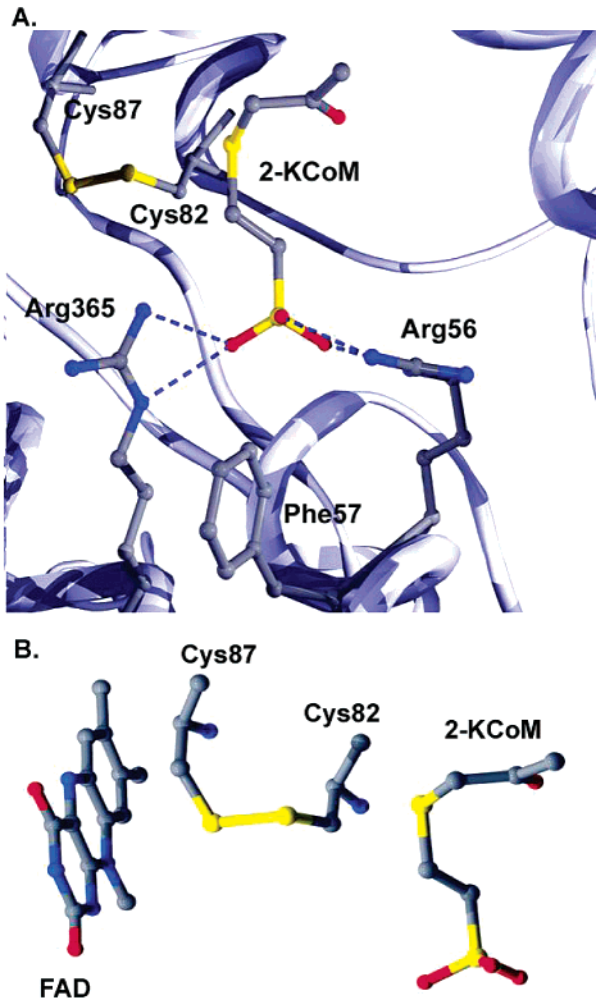

FIGURE 3: (A) Substrate binding at the active site highlighting the specific interactions with Arg side chains and the adjacent Phe residue. (B) Electron transfer pathway from FAD to the substrate sulfur atom of 2-ketopropyl-CoM.

binding domains. Although NADPH is not present in the current structure, the docking of NADPH into its binding site requires very little repositioning of amino acid side chains. The nicotinamide must be in close contact with the isoalloxazine moiety of FAD for direct hydride transfer from the C4 position of the nicotinamide ring to the N5 position of the isoalloxazine. The active site Cys82 and Cys87 residues form a disulfide bond (Figure 3A,B). Hydride transfer to FAD results in reduction of the enzyme disulfide via the presumed formation of a covalent adduct between the isoalloxazine at the C4A position and the proximal thiol of the reduced disulfide, by analogy to other members of the DOSR family (*16*). The resulting free thiol is then available for substrate thioether cleavage. The structure reveals a linear reduction pathway, and the modulation between oxidation and reduction of the redox active disulfide only requires changes in the conformation of the side chains of the active site Cys residues (Figure 3B). In this regard, the interchange thiol can be placed within bonding distance of the S of the substrate.

Stabilization of an Enolate Intermediate. In contrast to the specific side chain interactions observed for the substrate CoM moiety, the ketopropyl moiety is observed to have limited interactions with the protein. It was hypothesized that the presence of a hydrogen bond donor near the keto group of the substrate could serve to stabilize an enolate intermediate, facilitating the reductive cleavage of the thioether linkage analogous to bound Mg^{2+} observed in Rubisco (*38*). Although the electron density is not unambiguous with respect to the positioning of the ketopropyl moiety of the substrate, the best fit places the keto group of the substrate within hydrogen bonding distance of an ordered water molecule that is oriented by hydrogen bonding interactions with the peptide bond carbonyl of Leu78 and a side chain imidazole nitrogen of His137. The side chain of His137 is in turn oriented in its proper position by a specific interaction with the adjacent His84 (Figure 4A). The His-oriented water molecule could conceivably act as a proton donor for reaction with an enolacetone intermediate analogous to the enediol intermediate of ribulose 1,5-bisphosphate in Rubisco (*38*). The enolacetone intermediate provides an appropriate nucleophile for attack on the electrophilic carbon dioxide. The water molecule could also act in the stabilization of the intermediate as a hydrogen bond acceptor, serving a role analogous to that of Mg^{2+} in Rubisco (*38*). Since Mg^{2+} ion is isoelectronic with water, the assignment of water at this position is based on the coordination environment of this atom since the interaction of a His side chain nitrogen and a single peptide bond carbonyl would be an atypical coordination environment for Mg^{2+} ion. In addition, the results of previous biochemical studies indicate that Mg^{2+} is not required for 2-KPCC-catalyzed carboxylation, and its addition in enzyme assays does not stimulate activity (J. R. Allen and S. A. Ensign, unpublished results).

With the exception of the bound water molecule possibly involved in enolacetone formation and stabilization, the remaining environment of the ketopropyl moiety of the substrate is distinctly hydrophobic (Figure 4B). The interactions of the keto group with the His-bound water molecule serve to orient the methylene group which undergoes carboxylation toward the hydrophobic cavity. This water molecule is more than 5 Å from the methylene group of the ketopropyl moiety of the substrate and fixed in position by a hydrogen bonding interaction with both the His side chain, a peptide carbonyl, and the substrate keto group, perhaps making it an unlikely candidate as a proton donor for the reaction leading to acetone formation. Among these hydrophobic residues are two methionine residues which flank the CoM moiety of the substrate and act to shield the carboxylation site from the sulfonate moiety. An additional *cis*-amino acid conformation (Leu502) is observed in the substrate binding region, which allows the side chains of two hydrophobic residues, Phe501 and Leu502, to be oriented toward the substrate. Along these lines, a hallmark of other members of the DSOR family is the presence of a His side chain in the proximity of the interchange thiol to stabilize the thiol in the reduced state. The His at this position in 2-KPCC has been replaced with the side chain of Phe501, perhaps as an adaptation to eliminate the availability of protons to the reactive methylene group formed upon reductive cleavage.

Substrate-Induced Conformational Change. The distinctly hydrophobic nature of the active site could serve to exclude solvent interactions and thereby limit protonation of the enolate intermediate and formation of the undesired product acetone (Figure 1). Since in the substrate-bound form of the enzyme the substrate is virtually encapsulated in the protein,

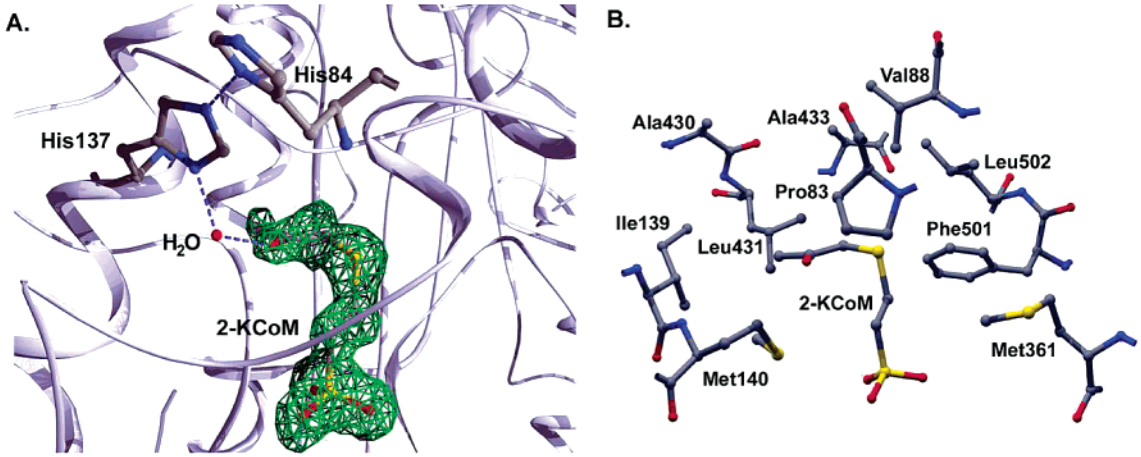

FIGURE 4: (A) Electron density maps ($2F_o - F_c$) contoured at 1σ about the substrate 2-ketopropyl-CoM showing His residues that are involved in orienting a water molecule that is located within hydrogen bonding distance of the substrate keto oxygen. (B) Amino acid residues that define the hydrophobic cavity surrounding the ketopropyl moiety of the substrate 2-ketopropyl-CoM.

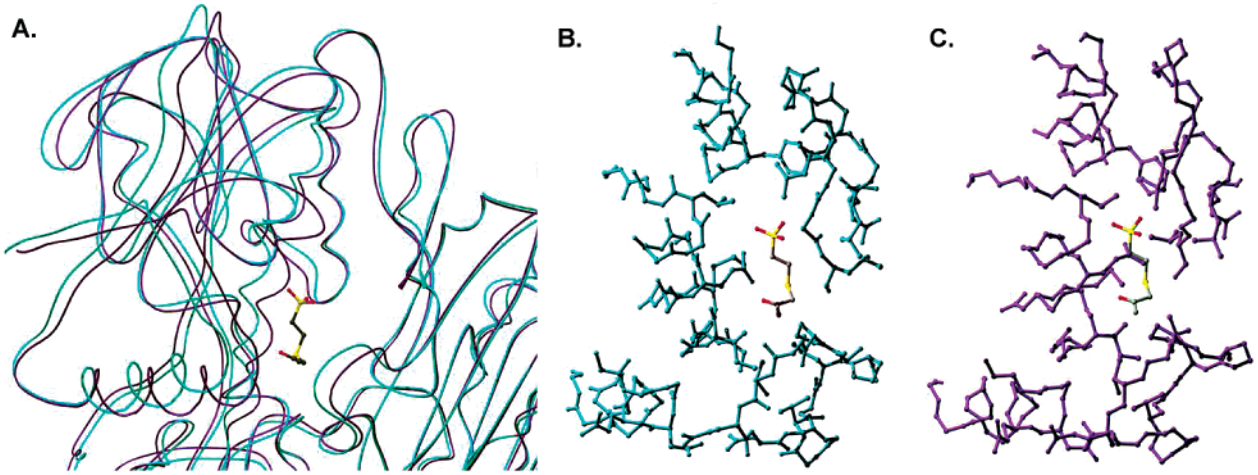

FIGURE 5: (A) Superimposition of the structure of native (cyan) and 2-ketopropyl-CoM-bound (purple) 2-KPCC showing the conformational changes induced upon substrate binding. The superimposition was accomplished as described by Kabsch (*43*) omitting regions of the N-terminus that undergo the largest conformational change in the superimposition. (B) Slab view of the substrate binding region of the native structure of 2-KPCC with the substrate 2-ketopropyl-CoM docked into the substrate binding site. (C) Analogous slab view of the substrate binding region in the substrate-bound form of 2-KPCC. The two views (B and C) depict the encapsulation of the substrate that occurs upon binding.

we have determined the structure of 2-KPCC in the absence of bound substrates in an effort to understand how substrate can be bound initially and how encapsulation is achieved. The structure of the native enzyme indicates that substrate access in 2-KPCC occurs through a well-defined channel directly opposite the NADPH binding cleft through a channel that is ~8 Å long and ~5 Å wide leading directly to the active site disulfide.

Comparison of the native and substrate-bound forms of the enzyme indicates that substrate binding brings about a conformational change as a likely result of the specific interactions of the CoM moiety of the substrate with the N-terminal region of the protein (Figure 5A). The main chain of the helical N-terminal region is displaced ~3.0 Å and results in additional conformational changes in the adjacent secondary structure elements within the FAD binding domain. The conformational change results in a collapse of the substrate binding channel, limiting access to the substrate binding site to only a narrow hydrophobic channel (Figure 5B,C). This manner of substrate sequestration is reminiscent of conformational changes observed in analogous comparisons of the high-resolution structures of native and substrate-bound states of spinach Rubisco in which movements of the N-terminal and C-terminal regions of Rubisco and a number of loop regions in concert encapsulate the substrate (*38*−*42*). These parallels are particularly interesting since Rubisco also catalyzes bond cleavage and carboxylation reactions in the conversion of Ribulose 1,5-bisphosphate and CO_2 to two molecules of 3-phosphoglycerate. Additionally, the results presented here may indicate a general mechanism whereby enzyme-bound enediol intermediates can be protected from interaction with the bulk solvent to avoid the formation of unproductive products.

The results described herein provide significant insight into how the prototypical reductive cleavage reactions catalyzed by the DSOR family of enzymes can be coordinated with a carboxylation reaction by a mechanism that is directly analogous to that of the canonical CO_2-fixing Rubisco.

REFERENCES

1. van Ginkel, C. G., and de Bont, J. A. M. (1986) *Arch. Microbiol. 145*, 403−407.

2. Habets-Crutzen, A. Q. H., Brink, L. E. S., van Ginkel, C. G., de Bont, J. A. M., and Tramper, J. (1984) *Appl. Microbiol. Biotechnol. 20*, 245−250.
3. Ensign, S. A. (2001) *Biochemistry 40*, 5846−5853.
4. Ensign, S. A., Small, F. J., Allen, J. R., and Sluis, M. K. (1998) *Arch. Microbiol. 169*, 179−187.
5. Small, F. J., and Ensign, S. A. (1997) *J. Bacteriol. 177*, 6170−6175.
6. Allen, J. R., and Ensign, S. A. (1998) *J. Bacteriol. 180*, 2072−2078.
7. Small, F. J., and Ensign, S. A. (1997) *J. Biol. Chem. 272*, 24913−24920.
8. Rosenzweig, A. C., Frederick, C. A., Lippard, S. J., and Nordlund, P. (1993) *Nature 366*, 537−543.
9. Allen, J. R., Clark, D. D., Krum, J. G., and Ensign, S. A. (1999) *Proc. Natl. Acad. Sci. U.S.A. 96*, 8432−8437.
10. Clark, D. D., Allen, J. R., and Ensign, S. A. (2000) *Biochemistry 39*, 1294−1304.
11. Allen, J. R., and Ensign, S. A. (1997) *J. Bacteriol. 179*, 3110−3115.
12. Swaving, J., de Bont, J. A. M., Westphal, A., and de Kok, A. (1996) *J. Bacteriol. 178*, 6644−6646.
13. Westphal, A. H., Swaving, J., Jacobs, L., and de Kok, A. (1998) *Eur. J. Biochem. 257*, 160−168.
14. Pai, E. F. (1991) *Curr. Opin. Struct. Biol. 1*, 796−803.
15. Mathews, F. S. (1991) *Curr. Opin. Struct. Biol. 1*.
16. Ghisla, S., and Massey, V. (1989) *Eur. J. Biochem. 181*, 1−17.
17. Williams, C. H., Jr. (1992) in *Chemistry and Biochemistry of Flavoproteins* (Muller, F., Ed.) pp 89, CRC Press, Boca Raton, FL.
18. Jang, S. B., Jeong, M. S., Clark, D. D., Ensign, S. A., and Peters, J. W. (2001) *Acta Crystallogr. D57*, 445−447.
19. Soltis, S. M., Stowell, M. H. B., Wiener, M. C., Phillips, G. N., and Rees, D. C. (1997) *J. Appl. Crystallogr. 30*, 190−194.
20. Leslie, A. G. W. (1992) in *Joint CCP4 and ESF-EACBM Newsletter on Protein Crystallography*, No. 26.
21. Otwinowski, Z., and Minor, W. (1997) *Methods in Enzymology* (Carter, C. W., Jr., and Sweet, R. M., Eds.) pp 20, Academic Press.
22. Collaborative Computational Project, No. 4 (1994) *Acta Crystallogr. D50*, 760−763.
23. Terwilliger, T. C., and Berendzen, J. (1999) *Acta Crystallogr. D55*, 849−861.
24. Jones, T. A., Zou, J. Y., Cowan, S. W., and Kjeldgaard, M. (1991) *Acta Crystallogr. A47*, 110−119.
25. Lamzin, V. S., and Perrakis, A. (2000) *Nat. Struct. Biol. 7*, 978−981.
26. Lamzin, V. S., Perrakis, A., Bricogne, G., Jiang, J., Swaminathan, S., and Sussman, J. L. (2000) *Acta Crystallogr. D56*, 1510−1511.
27. Brunger, A. T., Adams, P. D., Clore, G. M., DeLano, W. L., Gros, P., Grosse-Kunstleve, J. S., Jiang, J., Kuszewski, J., Nilges, M., Pannu, N. S., Read, R. J., Rice, L. M., Simonson, T., and Warren, G. L. (1998) *Acta Crystallogr. D54*, 905−921.
28. Brunger, A. T. (1992) *Nature 355*, 472−474.
29. Kissinger, D. K., Gehlhaar, D. K., and Fogel, D. B. (1999) *Acta Crystallogr. D55*, 484−491.
30. Laskowski, R. A., MacArthur, M. W., Moss, D. S., and Thornton, J. M. (1993) *J. Appl. Crystallogr. 26*, 283−291.
31. Guex, N., and Peitsch, M. C. (1997) *Electrophoresis 18*, 2714−2723.
32. Karplus, P. A., Pai, E. F., and Schulz, G. E. (1989) *Eur. J. Biochem. 178*, 693−703.
33. Karplus, P. A., and Schulz, G. E. (1987) *J. Mol. Biol. 195*, 701−729.
34. Pai, E. F., and Schulz, G. E. (1983) *J. Biol. Chem. 258*, 1751−1757.
35. Karplus, P. A., and Schulz, G. E. (1989) *J. Mol. Biol. 210*, 163−180.
36. Kuriyan, J., Kong, X.-P., Krishna, T. S. R., Sweet, R. M., Murgolo, N. J., Field, H., Cerami, A., and Henderson, G. B. (1991) *Proc. Natl. Acad. Sci. U.S.A. 88*, 8764−8768.
37. Schierbeek, A. J., Swarte, M. B. S., Dijkstra, B. W., Vriend, G., Read, R. J., Hol, W. G. J., Drenth, J., and Betzel, C. (1989) *J. Mol. Biol. 206*, 365−379.
38. Cleland, W. W., Andrews, T. J., Gutteridge, S., Hartman, F. C., and Lorimer, G. H. (1998) *Chem. Rev. 98*, 549−561.
39. Taylor, T. C., and Anderson, I. (1997) *J. Mol. Biol. 265*, 432.
40. Anderson, I. (1996) *J. Mol. Biol. 259*, 160−174.
41. Knight, S., Anderson, I., and Branden, C.-I. (1990) *J. Mol. Biol. 215*, 113.
42. Newman, J., and Gutteridge, S. J. (1993) *J. Biol. Chem. 268*, 25876.
43. Kabsch, W. (1976) *Acta Crystallogr. A32*, 922−923.

BI026580P